Field-induced decays in XXZ triangular-lattice antiferromagnets

P. A. Maksimov,[1] M. E. Zhitomirsky,[2] and A. L. Chernyshev[1]

[1]*Department of Physics and Astronomy, University of California, Irvine, California 92697, USA*
[2]*CEA, INAC-PHELIQS, F-38000, Grenoble, France*

(Dated: July 29, 2016)

We investigate field-induced transformations in the dynamical response of the XXZ model on the triangular lattice that are associated with the anharmonic magnon coupling and decay phenomena. A set of concrete theoretical predictions is made for a close physical realization of the spin-$\frac{1}{2}$ XXZ model, $Ba_3CoSb_2O_9$. We demonstrate that dramatic modifications in magnon spectrum must occur in low out-of-plane fields that are easily achievable for this material. The hallmark of the effect is a coexistence of the clearly distinct well-defined magnon excitations with significantly broadened ones in different regions of the $\mathbf{k}-\omega$ space. The field-induced decays are generic for this class of models and become more prominent at larger anisotropies and in higher fields.

PACS numbers: 75.10.Jm, 75.30.Ds, 75.50.Ee, 78.70.Nx

Triangular-lattice antiferromagnets (TLAFs) are central to the field of frustrated magnetism as representatives of one of the basic models epitomizing the effect of spin frustration [1–4]. They have attracted significant experimental and theoretical interest [5–21] as a potential source of spin-liquid and of a wide variety of intriguing ordered ground states, see Ref. [22]. Their spectral properties have recently emerged as a subject of intense research that has consistently uncovered broad, continuum-like spectral features [6, 23, 24], which are interpreted as an evidence of fractionalized excitations [6, 20, 25] or of the phenomenon of magnon decay [26–29].

In this work, we outline a theoretical proposal for a dramatic transformation of the spin-excitation spectrum of the XXZ triangular-lattice antiferromagnet in external out-of-plane field. This consideration pertains in particular to $Ba_3CoSb_2O_9$, one of the close physical realizations of the model that has recently been studied by a variety of experimental techniques [30–34]. The key finding of our work is that a modest out-of-plane field results in a strong damping of the high-energy magnons, affecting a significant part of the $\mathbf{k}$-space. This is different from a similar prediction of the field-induced decays in the square- and honeycomb-lattice AFs where strong spectrum transformations require large fields [35–38]. In the present case, because the staggered chirality of the field-induced umbrella spin structure breaks inversion symmetry, the resultant $\mathbf{k} \leftrightarrow -\mathbf{k}$ asymmetry of the magnon spectrum opens up a channel for decays of the high-energy magnons in a broad vicinity of the K$'$ corners of the Brillouin zone into the two-magnon continuum of the roton-like magnons at the K-points, see Fig. 1.

We note that the recent neutron-scattering work [23] asserts the existence of an intrinsic broadening in parts of the $Ba_3CoSb_2O_9$ spectrum even in zero field. While scatterings due to finite-temperature magnon population or strong effects of disorder in the non-collinear spin structures [39] cannot be ruled out as sources of damping observed in Ref. [23], we would like to point out that the phenomena discussed in this work are substantially more dramatic and should be free from such uncertainties.

Model and spectrum.—Owing to frustration and degeneracies of the model, triangular-lattice antiferromagnets in external field have a very rich phase diagram [40–43], featuring the hallmark plateau, coplanar, and umbrella states, see Ref. [22] for a recent review. We will focus on the XXZ Hamiltonian with an easy-plane anisotropy whose zero-field ground state is a 120° structure

$$\hat{\mathcal{H}} = J \sum_{\langle ij \rangle} \left(S_i^x S_j^x + S_i^y S_j^y + \Delta S_i^z S_j^z \right) - H \sum_i S_i^z, \quad (1)$$

where $\langle ij \rangle$ are nearest neighbor cites of the triangular lattice, $J > 0$, and $0 \le \Delta < 1$. In an out-of-plane magnetic field, the so-called umbrella structure is formed, see Fig. 1. In the isotropic limit, $\Delta = 1$, the coplanar states are favored instead, but $\Delta < 1$ always stabilizes the semiclassical umbrella state for a range of fields, with the $H - \Delta$ region of its stability for $S = 1/2$ sketched in

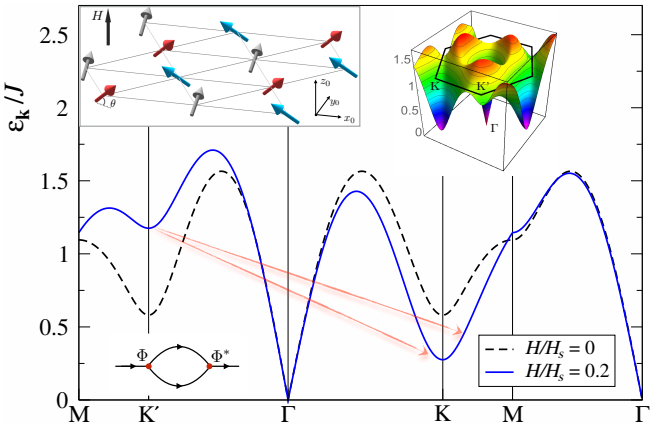

FIG. 1: Linear spin wave energy $\varepsilon_{\mathbf{k}}$ of model (1) for $\Delta = 0.9$, $S = 1/2$ and the fields $H = 0$ and $H = 0.2H_s$. Arrows show schematics of the decay. Insets: umbrella structure in a field, 3D plot of $\varepsilon_{\mathbf{k}}$ for $H = 0.2H_s$, and decay self-energy diagram.

Fig. 2(c) [from Ref. [43]]. In $Ba_3CoSb_2O_9$, estimates of the anisotropy yield $\Delta \approx 0.9$ [23, 33] with an additional stabilization of the umbrella-like state provided by the interplane coupling [34, 44]. The linear spin-wave (LSW) treatment of the model (1) within the $1/S$-expansion is standard, see [45]. The harmonic magnon energies, $\varepsilon_{\mathbf{k}}$, are depicted in Fig. 1 for $S=1/2$, $\Delta=0.9$, and $H=0$ and $H=0.2H_s$, where $H_s=6JS(\Delta+1/2)$ is the saturation field. The chosen representative field of $0.2H_s$ is within the umbrella region of Fig. 2(c) and for $Ba_3CoSb_2O_9$ it corresponds a modest field of about 6 T [33].

In Fig. 1, one can see the gaps $\propto\sqrt{1-\Delta}$ at K and K′ points in zero field. In a finite field, the staggered scalar chirality of the umbrella structure, $\mathbf{S}_i\cdot(\mathbf{S}_j\times\mathbf{S}_k)$, induces inversion symmetry breaking. Because of that, magnon energy acquires an asymmetric contribution [46], $\varepsilon_{\mathbf{k}}\neq\varepsilon_{-\mathbf{k}}$, with the energies at K (K′) points lowered (raised) proportionally to the field. Note that the K and K′ points trade their places in the domain with a shifted pattern of the 120° order that also corresponds to the flipped staggered chiralities. It is clear, that the distorted band structure brings down the energy of a minimum of the two-magnon continuum associated with the low-energy, roton-like magnons at K-points. Given the remaining commensurability of the umbrella state, which retains the $3\mathbf{K}=0$ property of the 120° structure, magnon decays may occur in a proximity of the K′ points via a process $\varepsilon_{\mathbf{K}'}\Rightarrow\varepsilon_{\mathbf{K}}+\varepsilon_{\mathbf{K}(\pm\mathbf{G}_i)}$, where $\mathbf{G}_i$'s are the reciprocal lattice vectors. While the exact kinematics of such decays is somewhat more complicated, one can simply check where and at what field the on-shell decay conditions, $\varepsilon_{\mathbf{k}}=\varepsilon_{\mathbf{q}}+\varepsilon_{\mathbf{k}-\mathbf{q}}$, are first met for a given Δ.

This direct verification yields the lower border of the shaded regions in Fig. 2(c), which is a union of three curves. At large anisotropies, $\Delta\to 0$, the decay conditions that are fulfilled at the lowest field are the ones associated with the change of the curvature of the Goldstone mode near the Γ point, the kinematics familiar from the field-induced decays in the square-lattice [35] and honeycomb-lattice AFs [38], as well as ^{4}He [47]. At larger Δ, the threshold field for decays is precisely determined by the "asymmetry-induced" condition $\varepsilon_{\mathbf{K}'}=2\varepsilon_{\mathbf{K}}$ discussed above, which is given analytically by $H^*=\sqrt{(1-\Delta)/(13-\Delta)}$ and is shown by the dashed line in Fig. 2(c). Closer to the isotropic limit, $\Delta\gtrsim 0.7$, the decay conditions are first met away from the high-symmetry points, see some discussion of them for the zero-field case and $\Delta>0.92$ in Ref. [28].

On(off)-shell decay rate.—To get a sense of the quantitative measure of the field-induced broadening effect and of the extent of the affected $\mathbf{k}$-space, we first present the results for the decay rate in the Born approximation

$$\Gamma_{\mathbf{k}}=\Gamma_0\sum_{\mathbf{q}}|\Phi_{\mathbf{q},\mathbf{k}-\mathbf{q};\mathbf{k}}|^2\,\delta\left(\omega_{\mathbf{k}}-\omega_{\mathbf{q}}-\omega_{\mathbf{k}-\mathbf{q}}\right), \qquad (2)$$

where $\Gamma_0=3\pi J/4$ and $\varepsilon_{\mathbf{k}}=3JS\omega_{\mathbf{k}}$. The three-magnon

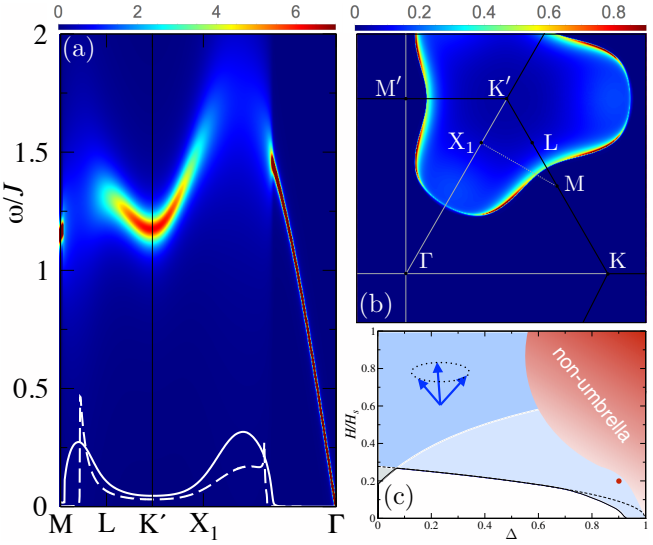

FIG. 2: (a) The intensity plot of the spectral function along MK′Γ path with $\Gamma_{\mathbf{k}}$ from the self-consistent iDE for $\Delta=0.9$ and $H=0.2H_s$. Dashed and solid lines are $\Gamma_{\mathbf{k}}$ in the Born approximation (2) and the iDE solution. (b) The 2D intensity plot of $\Gamma_{\mathbf{k}}$ from (2). (c) The $H-\Delta$ diagram of the decay thresholds in the umbrella state. Shaded are the regions where various forms of decay are allowed, see text. The non-umbrella region for $S=1/2$ is sketched from Ref. [43]. The dot marks the values of Δ and H used in (a) and (b).

decay vertex $\Phi_{\mathbf{q},\mathbf{k}-\mathbf{q};\mathbf{k}}$ is derived from the anharmonic coupling terms of the $1/S$-expansion of the model (1), see [45]. It combines the effects of noncollinearity due to in-plane 120° structure and of the field-induced tilting of spins [26, 28, 35]. We show $\Gamma_{\mathbf{k}}$ for a representative $H=0.2H_s$ and for the same $\Delta=0.9$ and $S=1/2$ as above: in Fig. 2(a) along the MK′Γ path (dashed line) and in Fig. 2(b) as a 2D intensity plot.

In addition, we also present the results of the self-consistent solution of the off-shell Dyson's equation (DE) for $\Gamma_{\mathbf{k}}$, in which corrections to the magnon energy are ignored but the imaginary part of the the magnon self-energy $\Sigma_{\mathbf{k}}(\omega)$ due to three-magnon coupling is retained, referred to as the iDE approach: $\Gamma_{\mathbf{k}}=-\mathrm{Im}\,\Sigma_{\mathbf{k}}\left(\varepsilon_{\mathbf{k}}+i\Gamma_{\mathbf{k}}\right)$. This method accounts for a damping of the decaying initial-state magnon and regularizes the van Hove singularities associated with the two-magnon continuum that can be seen in the Born results of (2) in Fig. 2(a). The same Figure shows the iDE results for $\Gamma_{\mathbf{k}}$ (solid line) and the corresponding magnon spectral function in a lorentzian form (intensity plot). We note that the self-consistency schemes that rely on the broadening of the decay products, such as iSCBA discussed in Refs. [36, 48], are not applicable here because the final-state magnons remain well-defined in our case. Altogether, our consideration suggests that a significant field-induced broadening of quasiparticle peaks due to magnon decays should appear in a wide vicinity of the K′ points in low fields.

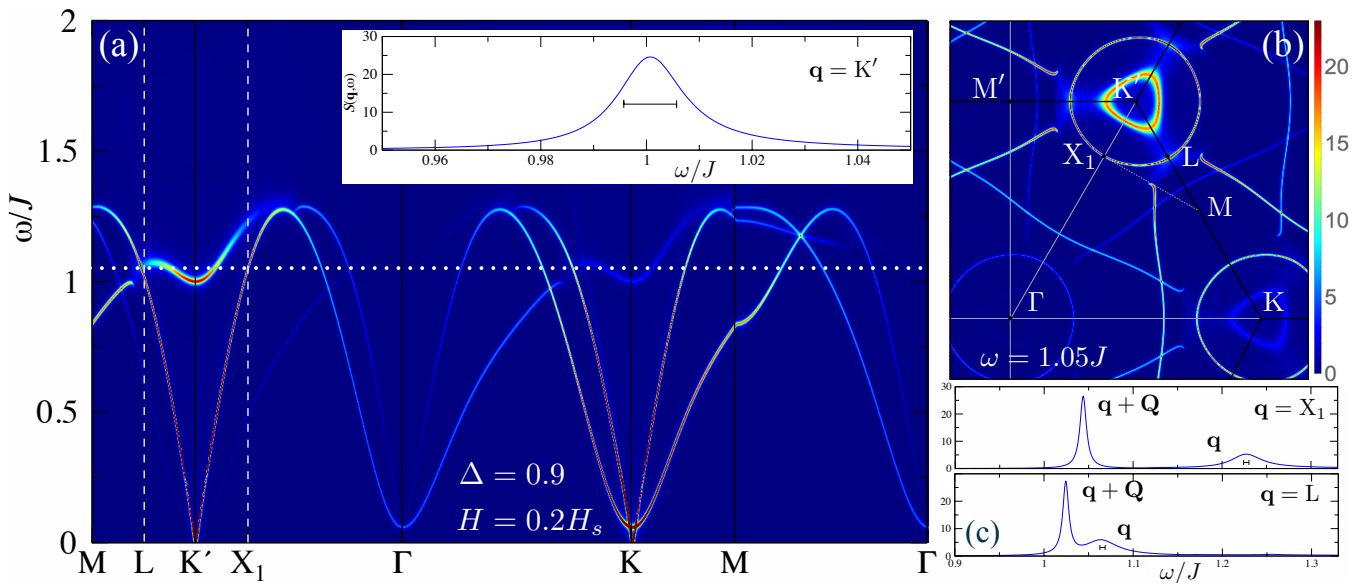

FIG. 3: (a) Intensity plot of $\mathcal{S}(\mathbf{q},\omega)$ along the MK′ΓKMΓ path. Dotted and dashed lines are constant-energy cut in (b) and ω-cuts in (c). Inset: $\mathcal{S}(\mathbf{q},\omega)$ vs ω at K′. Bars are artificial width $2\delta=0.01J$ of the calculation [52]. $S=1/2$, $\Delta=0.9$, $H=0.2H_s$.

Dynamical structure factor.—Next, we evaluate the dynamical spin-spin structure factor $\mathcal{S}(\mathbf{q},\omega)$, the quantity directly observed in the inelastic neutron scattering experiments. Following Ref. [29], we approximate $\mathcal{S}(\mathbf{q},\omega)$ as a sum of the diagonal terms [45] of

$$\mathcal{S}^{\alpha_0\beta_0}(\mathbf{q},\omega)=\frac{i}{\pi}\mathrm{Im}\int_{-\infty}^{\infty}dt e^{i\omega t}\langle T S^{\alpha_0}_{\mathbf{q}}(t)S^{\beta_0}_{-\mathbf{q}}(0)\rangle. \quad (3)$$

Transforming to the local (rotating) reference frame of the ordered moments and keeping terms that contribute to the leading $1/S$ order [29] yields

$$\mathcal{S}^{x_0x_0}(\mathbf{q},\omega)=\frac{1}{4}\Big[\mathcal{S}^{yy}_{\mathbf{q}+}+\mathcal{S}^{yy}_{\mathbf{q}-}-2i\sin\theta\left(\mathcal{S}^{xy}_{\mathbf{q}+}-\mathcal{S}^{xy}_{\mathbf{q}-}\right)$$
$$+\sin^2\theta\left(\mathcal{S}^{xx}_{\mathbf{q}+}+\mathcal{S}^{xx}_{\mathbf{q}-}\right)+\cos^2\theta\left(\mathcal{S}^{zz}_{\mathbf{q}+}+\mathcal{S}^{zz}_{\mathbf{q}-}\right)\Big], \quad (4)$$
$$\mathcal{S}^{z_0z_0}(\mathbf{q},\omega)=\cos^2\theta\,\mathcal{S}^{xx}_{\mathbf{q}}+\sin^2\theta\,\mathcal{S}^{zz}_{\mathbf{q}},$$

and $\mathcal{S}^{y_0y_0}(\mathbf{q},\omega)=\mathcal{S}^{x_0x_0}(\mathbf{q},\omega)$. Here we used the antisymmetric nature of the xy contribution $\mathcal{S}^{xy}_{\mathbf{q}}=-\mathcal{S}^{yx}_{\mathbf{q}}$ and introduced shorthand notations for $\mathcal{S}^{\alpha\beta}_{\mathbf{q}}\equiv\mathcal{S}^{\alpha\beta}(\mathbf{q},\omega)$ and "shifted" momenta $\mathbf{q}\pm\equiv\mathbf{q}\pm\mathbf{K}$, with θ being the out-of-plane canting angle of spins. In the local reference frame, $\mathcal{S}^{zz}_{\mathbf{q}}$ components of the dynamical structure factor are "longitudinal", i.e., are due to the two-magnon continuum, having no sharp quasiparticle features [29]. The rest of Eq. (4) is "transverse", i.e., is related to the single-magnon spectral function, $\mathcal{S}^{x(y)x(y)}_{\mathbf{q}}\propto A(\mathbf{q},\omega)$, with different kinematic $\mathbf{q}$-dependent formfactors, where $A(\mathbf{q},\omega)=-(1/\pi)\mathrm{Im}G(\mathbf{q},\omega)$ and the diagonal magnon Green's function is $G(\mathbf{q},\omega)=[\omega-\varepsilon_{\mathbf{q}}-\Sigma_{\mathbf{q}}(\omega)+i\delta]^{-1}$. Thus, the dynamical structure factor of the XXZ TLAF in a field should feature three overlapping single-magnon spectral functions, $A(\mathbf{q},\omega)$ and $A(\mathbf{q}\pm\mathbf{K},\omega)$, with different weights according to (4) and [45], see also [49].

In our consideration, we include all contributions to the one-loop magnon self-energy $\Sigma_{\mathbf{q}}(\omega)$ of the $1/S$-order of the non-linear spin-wave theory [26]. Namely, there are two more terms in addition to decay diagram: the source diagram and the Hartree-Fock correction, the latter comprised of the contributions from the four-magnon interactions (quartic terms) and from the quantum corrections to the out-of-plane canting angle of spins, see [45] for technical details,

$$\Sigma_{\mathbf{q}}(\omega)=\Sigma^{\mathrm{HF}}_{\mathbf{q}}+\Sigma^{d}_{\mathbf{q}}(\omega)+\Sigma^{s}_{\mathbf{q}}(\omega). \quad (5)$$

Having included all one-loop contributions also allows us to consistently take into account the ω-dependence of the magnon spectral function. Below we demonstrate that anharmonic interactions lead to broadening of magnon quasiparticle peaks, redistribution of spectral weight, and other dramatic changes in the spectrum.

In Fig. 3, we present our results for the dynamical structure factor $\mathcal{S}(\mathbf{q},\omega)$ in (4) of the model (1) for $S=1/2$, $\Delta=0.9$, and $H=0.2H_s$. First, there is a strong downward bandwidth renormalization by about 30% compared to the LSW results in Fig. 1, which is characteristic to the TLAFs [18, 27, 28]. The most important result is a significant broadening of magnon spectra for an extensive range of momenta, accompanied by well-pronounced termination points with distinctive bending of spectral lines [51] and other non-Lorentzian features that are associated with crossings of the two-magnon continuum. The broadening can be seen in a wide proximity of the K′ points of the Brillouin zone as well as in the equivalent regions of the "±**K**-shifted" components

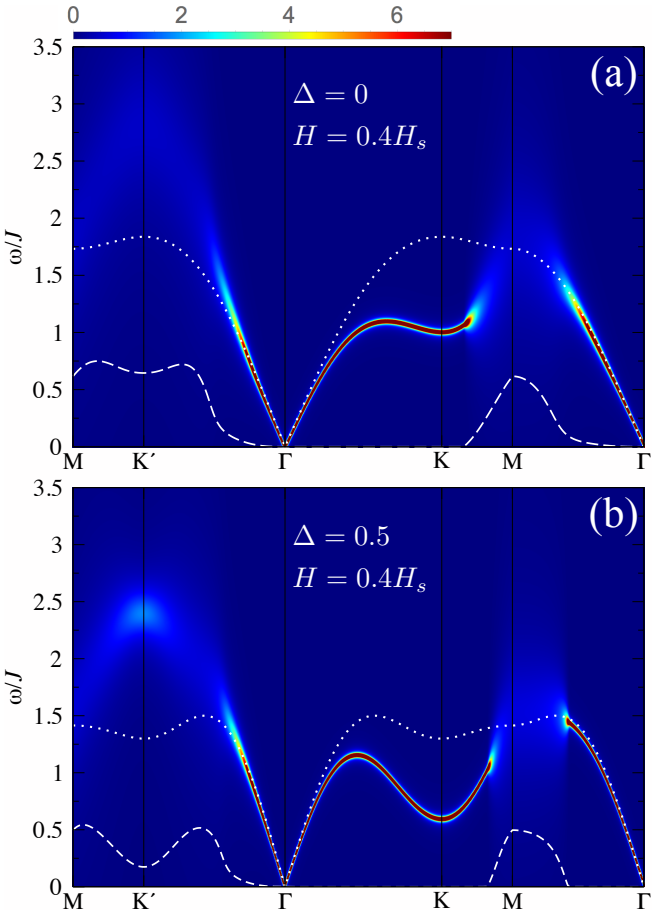

FIG. 4: Intensity plots of the spectral function with the iDE $\Gamma_{\mathbf{k}}$ (dashed lines) for $S=1/2$, $H=0.4H_s$, and $\Delta=0$ in (a) and $\Delta=0.5$ in (b). Dotted lines are the LSW spectra for $H=0$.

of the structure factor. Despite the strong renormalization of the spectrum, the extent of the affected $\mathbf{q}$-region is about the same as in the on-shell consideration in Fig. 2.

The inset of Fig. 3(a) shows $\mathcal{S}(\mathbf{q},\omega)$ vs ω at a representative K$'$ point that exhibits a modest broadening compared with the artificial width (2δ) of the calculation. The ω-cuts at the X_1 and L points near the boundaries of the decay region in Fig. 3(c) show much heavier damping in one of the component of $\mathcal{S}(\mathbf{q},\omega)$, which coexists with the well-defined spectral peak from the "shifted" component. The enhancement of magnon decays near the edge of decay region also correlates well with the on-shell results in Fig. 2 and points to the van Hove singularities of the two-magnon continuum as a culprit. The 2D intensity map of the constant-energy cut of $\mathcal{S}(\mathbf{q},\omega)$ at $\omega=1.05J$ is shown in Fig. 3(b), where one can see multiple signatures of the broadening, spectral weight redistribution around K$'$, and termination points.

Larger anisotropy.—We complement our consideration of the model (1) by demonstrating the effects of magnetic field on the magnon spectrum for the TLAFs with large easy-plane anisotropy. In the strongly-anisotropic limit, $\Delta=0$, the non-linear anharmonic coupling of magnons is known to result in a very strong spectrum renormalization (about 50%), but with no decays kinematically allowed [28]. For $S=1/2$ and small enough Δ, Born approximation and the $1/S$, one-loop, ω-dependent self-energy approach are somewhat inconsistent in that the first produces unphysically large $\Gamma_{\mathbf{k}}$ for $H\gtrsim 0.3H_s$ and the second shows strong spectrum renormalization that avoids decays for $H\lesssim 0.5H_s$. Since the reason for this discrepancy is the lack of self-consistency, we resort to the (partially) self-consistent iDE approach described above. In Fig. 4, we show its results for the magnon spectral function with the Lorentzian broadening $\Gamma_{\mathbf{k}}$ for $\Delta=0$ and $\Delta=0.5$ and for $H=0.4H_s$. What is remarkable is not only a persistent pattern of a wide $\mathbf{k}$-region of the strongly overdamped high-energy magnons [cf., Fig. 2(a)], but also the magnitudes of their broadening, which reach the values of almost a half of the magnon bandwidth even after a self-consistent regularization.

Conclusions.—We have provided a detailed analysis of the field-induced dynamical response of the XXZ model on the triangular lattice within the umbrella phase. We have demonstrated a ubiquitous presence of significant damping of the high-energy magnons already in moderate fields, $H\gtrsim 0.2H_s$. Other characteristic features, such as significant spectral weight redistribution and termination points that separate well-defined excitations from the ones that are overdamped, are also expected to occur. The key physical ingredients of this dramatic spectral transformation are a strong spin noncollinearity, which is retained by the umbrella state and is essential for the anharmonic magnon coupling and decays, and the tilted, $\mathbf{k}\leftrightarrow-\mathbf{k}$ asymmetric magnon band structure, owing its origin to the staggered chirality of the umbrella state that breaks the inversion symmetry. Our consideration pertains in particular to $Ba_3CoSb_2O_9$, which is currently a prime candidate for observing aforementioned properties in reasonably small fields reachable in experimental setup. Our work should be of a qualitative and quantitative guidance for observations of the dynamical structure factor in the inelastic neutron-scattering experiments in this and other related systems.

Acknowledgments.—We acknowledge useful conversations with Martin Mourigal and Cristian Batista. We are particularly indebted to Martin for his unbiased experimental intuition that led to [49]. This work was supported by the U.S. Department of Energy, Office of Science, Basic Energy Sciences under Award # DE-FG02-04ER46174. A. L. C. would like to thank the Kavli Institute for Theoretical Physics where part of this work was done. The work at KITP was supported in part by NSF Grant No. NSF PHY11-25915.

[1] G. H. Wannier, Phys. Rev. **79**, 357 (1950).

[2] P. W. Anderson, Mater. Res. Bull. **8**, 153 (1973); P. Fazekas and P. W. Anderson, Philos. Mag. **30**, 423 (1974).
[3] D. A. Huse and V. Elser, Phys. Rev. Lett. **60**, 2531 (1988).
[4] D. H. Lee, J. D. Joannopoulos, J. W. Negele, and D. P. Landau, Phys. Rev. Lett. **52**, 433 (1984).
[5] M. F. Collins and O. A. Petrenko, Canad. J. Phys. **75**, 605 (1997).
[6] R. Coldea, D. A. Tennant, A. M. Tsvelik, and Z. Tylczynski, Phys. Rev. Lett. **86**, 1335 (2001); R. Coldea, D. A. Tennant, K. Habicht, P. Smeibidl, C. Wolters, and Z. Tylczynski, Phys. Rev. Lett. **88**, 137203 (2002).
[7] L. E. Svistov, A. I. Smirnov, L. A. Prozorova, O. A. Petrenko, L. N. Demianets, and A. Ya. Shapiro, Phys. Rev. B **67**, 094434 (2003).
[8] S. Nakatsuji, Y. Nambu, H. Tonomura, O. Sakai, S. Jonas, C. Broholm, H. Tsunetsugu, Y. Qiu, and Y. Maeno, Science **309**, 1697 (2005).
[9] A. Olariu, P. Mendels, F. Bert, B. G. Ueland, P. Schiffer, R. F. Berger, and R. J. Cava, Phys. Rev. Lett. **97**, 167203 (2006).
[10] T. Oguchi, J. Phys. Soc. Jpn. Suppl. **52**, 183 (1983).
[11] Th. Jolicoeur and J. C. Le Guillou, Phys. Rev. B **40**, 2727 (1989).
[12] S. J. Miyake, J. Phys. Soc. Jpn. **61**, 983 (1992).
[13] A. V. Chubukov, S. Sachdev, and T. Senthil, J. Phys. Condens. Matter **6**, 8891 (1994).
[14] P. W. Leung and K. J. Runge, Phys. Rev. B **47**, 5861 (1993).
[15] B. Bernu, P. Lecheminant, C. Lhuillier, and L. Pierre, Phys. Rev. B **50**, 10048 (1994).
[16] L. Capriotti, A. E. Trumper, and S. Sorella, Phys. Rev. Lett. **82**, 3899 (1999).
[17] Z. Weihong, J. Oitmaa, and C. J. Hamer, Phys. Rev. B **44**, 11869 (1991).
[18] W. Zheng, J. O. Fjærestad, R. R. P. Singh, R. H. McKenzie, and R. Coldea, Phys. Rev. B **74**, 224420 (2006).
[19] S. R. White and A. L. Chernyshev, Phys. Rev. Lett. **99**, 127004 (2007).
[20] O. A. Starykh, H. Katsura, and L. Balents, Phys. Rev. B **82**, 014421 (2010).
[21] Z. Zhu and S. R. White, Phys. Rev. B **92**, 041105 (2015).
[22] O. A. Starykh, Rep. Prog. Phys. **78**, 052502 (2015).
[23] J. Ma, Y. Kamiya, T. Hong, H. B. Cao, G. Ehlers, W. Tian, C. D. Batista, Z. L. Dun, H. D. Zhou, and M. Matsuda, Phys. Rev. Lett. **116**, 087201 (2016).
[24] J. Oh, M. D. Le, J. Jeong, J. Lee, H. Woo, W.-Y. Song, T. G. Perring, W. J. L. Buyers, S.-W. Cheong, and J.-G. Park, Phys. Rev. Lett. **111**, 257202 (2013).
[25] E. A. Ghioldi, A. Mezio, L. O. Manuel, R. R. P. Singh, J. Oitmaa, and A. E. Trumper, Phys. Rev. B **91**, 134423 (2015).
[26] M. E. Zhitomirsky and A. L. Chernyshev, Rev. Mod. Phys. **85**, 219 (2013).
[27] O. A. Starykh, A. V. Chubukov, and A. G. Abanov, Phys. Rev. B **74**, 180403 (2006).
[28] A. L. Chernyshev and M. E. Zhitomirsky, Phys. Rev. Lett. **97**, 207202 (2006); Phys. Rev. B **79**, 144416 (2009).
[29] M. Mourigal, W. T. Fuhrman, A. L. Chernyshev, and M. E. Zhitomirsky, Phys. Rev. B **88**, 094407 (2013).
[30] Y. Doi, Y. Hinatsu, and K. Ohoyama, J. Phys.: Condens. Matter **16**, 8923 (2004).
[31] Y. Shirata, H. Tanaka, A. Matsuo, and K. Kindo, Phys. Rev. Lett. **108**, 057205 (2012).
[32] H. D. Zhou, C. Xu, A. M. Hallas, H. J. Silverstein, C. R. Wiebe, I. Umegaki, J. Q. Yan, T. P. Murphy, J.-H. Park, Y. Qiu, J. R. D. Copley, J. S. Gardner, and Y. Takano, Phys. Rev. Lett. **109**, 267206 (2012).
[33] T. Susuki, N. Kurita, T. Tanaka, H. Nojiri, A. Matsuo, K. Kindo, and H. Tanaka, Phys. Rev. Lett. **110**, 267201 (2013).
[34] G. Koutroulakis, T. Zhou, Y. Kamiya, J. D. Thompson, H. D. Zhou, C. D. Batista, and S. E. Brown, Phys. Rev. B **91**, 024410 (2015).
[35] M. E. Zhitomirsky and A. L. Chernyshev, Phys. Rev. Lett. **82**, 4536 (1999).
[36] M. Mourigal, M. E. Zhitomirsky, and A. L. Chernyshev, Phys. Rev. B **82**, 144402 (2010).
[37] W. T. Fuhrman, M. Mourigal, M. E. Zhitomirsky, and A. L. Chernyshev, Phys. Rev. B **85**, 184405 (2012).
[38] P. A. Maksimov and A. L. Chernyshev, Phys. Rev. B **93**, 014418 (2016).
[39] W. Brenig and A. L. Chernyshev, Phys. Rev. Lett. **110**, 157203 (2013).
[40] H. Kawamura and S. Miyashita, J. Phys. Soc. Jpn. **54**, 4530 (1985).
[41] S. E. Korshunov, J. Phys. C: Solid State Phys. **19**, 5927 (1986).
[42] A. V. Chubukov and D. I. Golosov, J. Phys.: Condens. Matter **3**, 69 (1991).
[43] D. Yamamoto, G. Marmorini, and I. Danshita, Phys. Rev. Lett. **112**, 127203 (2014); G. Marmorini, D. Yamamoto, and I. Danshita, Phys. Rev. B **93**, 224402 (2016).
[44] R. S. Gekht and I. N. Bondarenko, J. Exp. Theor. Phys. **84**, 345 (1997).
[45] See Supplemental Material at http://link.aps.org/supplemental/, for details on the non-linear spin-wave theory.
[46] M. E. Zhitomirsky and I. A. Zaliznyak, Phys. Rev. B **53**, 3428 (1996).
[47] L.P. Pitaevskii, Zh. Eksp. Teor. Fiz. **36**, 1168 (1959) [Sov. Phys. JETP **9**, 830 (1959)].
[48] T. J. Sluckin and R. M. Bowley, J. Phys. C: Solid State Phys. **7**, 1779 (1974).
[49] In experimental systems, one may expect that domains with opposite patterns of staggered chiralities are present. In that case, the dynamical structure factor $\mathcal{S}(\mathbf{q},\omega)$ is a superposition of Fig. 3 and its mirror image. The single-domain chiral order can be produced, e.g., by the magnetoelectric effect [50].
[50] M. Mourigal, M. Enderle, R. K. Kremer, J. M. Law, and B. Fåk, Phys. Rev. B **83**, 100409 (2011).
[51] K. W. Plumb, K. Hwang, Y. Qiu, L. W. Harriger, G. E. Granroth, A. I. Kolesnikov, G. J. Shu, F. C. Chou, C. Rüegg, Y. B. Kim, and Y.-J. Kim, Nat. Phys. **12**, 224 (2016).
[52] Calculations of the self-energy $\Sigma_{\mathbf{k}}(\omega)$ were performed with a smaller artificial broadening $\delta' = 0.0005J$.

Field-induced decays in XXZ triangular-lattice antiferromagnets: Supplemental Material

P. A. Maksimov[1], M. E. Zhitomirsky[2], and A. L. Chernyshev[1]

[1] *Department of Physics and Astronomy, University of California, Irvine, California 92697, USA*
[2] *CEA, INAC-PHELIQS, F-38000, Grenoble, France*

(Dated: July 27, 2016)

Here we present the details of the nonlinear spin-wave formalism for the XXZ model on a triangular lattice in an out-of-plane magnetic field and in the semi-classical umbrella state. The formalism bears significant similarities to the Heisenberg triangular antiferromagnet case in zero field [1, 2] and to the square-lattice antiferromagnet in a field [3], with several details that differ from both.

Model and spin transformation

The nearest-neighbor XXZ Hamiltonian on a triangular lattice in external out-of-plane field is

$$\hat{\mathcal{H}} = J\sum_{\langle ij\rangle}\left(\mathbf{S}_i\cdot\mathbf{S}_j - (1-\Delta)\,S_i^{z_0}S_j^{z_0}\right) - H\sum_i S_i^{z_0}\ , \quad (1)$$

where the sum is over the nearest-neighbor bonds $\langle ij\rangle$, $J>0$ is an exchange coupling constant, $0\le\Delta\le 1$ is the easy-plane anisotropy parameter, and H is external magnetic field in units of $g\mu_B$. The ground state in zero field is a 120° structure with the ordering vector $\mathbf{Q}=\left(\frac{4\pi}{3},0\right)$. In applied field, spins cant towards the field direction to form the umbrella structure shown in Fig. 1. Thus, we need to align the local spin-quantization axis on each site in the direction given by the spin configuration, with the canting angle defined from the energy minimization.

The corresponding general transformation of the spin components from the laboratory reference frame $\{x_0,y_0,z_0\}$ to the local reference frame $\{x,y,z\}$ can be performed using two consequent rotations

$$\mathbf{S}_i^0 = \mathbf{R}_\mathbf{Q}\cdot\mathbf{R}_\theta\cdot\mathbf{S}_i\,, \quad (2)$$

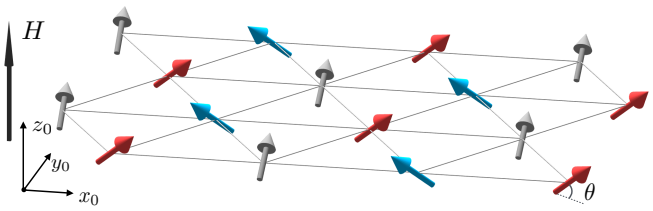

FIG. 1: Umbrella spin structure on the triangular lattice, θ is the out-of-plane canting angle.

where the matrix $\mathbf{R}_\mathbf{Q}$ does rotations in the $\{x_0y_0\}$-plane

$$\mathbf{R}_\mathbf{Q} = \begin{pmatrix} \cos\varphi_i & -\sin\varphi_i & 0\\ \sin\varphi_i & \cos\varphi_i & 0\\ 0 & 0 & 1\end{pmatrix}, \quad (3)$$

where $\varphi_i=\mathbf{Q}\cdot\mathbf{r}_i$ is an in-plane angle. The out-of-plane rotation is done by $\mathbf{R}_\theta$ within the $\{x_0,z_0\}$-plane

$$\mathbf{R}_\theta = \begin{pmatrix} \sin\theta & 0 & \cos\theta\\ 0 & 1 & 0\\ -\cos\theta & 0 & \sin\theta\end{pmatrix}, \quad (4)$$

where θ is the out-of-plane canting angle. The full transformation is explicitly given by

$$\begin{aligned} S^{x_0} &= S^x\sin\theta\cos\mathbf{Q}\cdot\mathbf{r} - S^y\sin\mathbf{Q}\cdot\mathbf{r} + S^z\cos\theta\cos\mathbf{Q}\cdot\mathbf{r},\\ S^{y_0} &= S^x\sin\theta\sin\mathbf{Q}\cdot\mathbf{r} + S^y\cos\mathbf{Q}\cdot\mathbf{r} + S^z\cos\theta\sin\mathbf{Q}\cdot\mathbf{r},\\ S^{z_0} &= -S^x\cos\theta + S^z\sin\theta. \end{aligned} \quad (5)$$

Transformed Hamiltonian

After performing the axis-rotation transformation (2), we split Hamiltonian into "even" and "odd" parts

$$\hat{\mathcal{H}} = \hat{\mathcal{H}}_{\rm even} + \hat{\mathcal{H}}_{\rm odd}\,, \quad (6)$$

which become even and odd in bosonic field operators

$$\begin{aligned} \hat{\mathcal{H}}_{\rm even} = J\sum_{\langle ij\rangle} & S_i^xS_j^x\left[\sin^2\theta\cos\delta\varphi_{ij} + \Delta\cos^2\theta\right]\\ & + S_i^yS_j^y\cos\delta\varphi_{ij}\\ & + S_i^zS_j^z\left[\cos^2\theta\cos\delta\varphi_{ij} + \Delta\sin^2\theta\right]\\ & + \left(S_i^xS_j^y - S_i^yS_j^x\right)\sin\delta\varphi_{ij}\sin\theta\\ & - H\sum_i S_i^z\sin\theta. \end{aligned} \quad (7)$$

Within the $1/S$ expansion, this term will yield classical energy, harmonic spectrum, and four-magnon interactions. The three-magnon interactions will be produced by the odd Hamiltonian and originate from the non-collinear spin structure

$$\begin{aligned} \hat{\mathcal{H}}_{\rm odd} = J\sum_{\langle ij\rangle} & \left(S_i^xS_j^z + S_i^zS_j^x\right)\sin\theta\cos\theta\left(-\Delta+\cos\delta\varphi_{ij}\right)\\ & + \left(S_i^zS_j^y - S_i^yS_j^z\right)\cos\theta\sin\delta\varphi_{ij}\\ & + \sum_i HS_i^x\cos\theta, \end{aligned} \quad (8)$$

where $\delta\varphi_{ij} = \varphi_i - \varphi_j = \pm 120^\circ$, i.e., the in-plane spin configuration is retained in the umbrella state. The classical energy can be obtained from (7) as

$$\frac{E_{\rm cl}}{NJS^2} = 3\Big(\Delta \sin^2\theta - \frac{1}{2}\cos^2\theta\Big) - \frac{H\sin\theta}{JS}\,, \qquad (9)$$

with the minimization yielding a relation between the field H and the canting angle θ as: $H = H_s \sin\theta$ where $H_s = 6JS\left(\Delta + \frac{1}{2}\right)$ is the saturation field. The subsequent treatment of the spin Hamiltonian in (7) and (8) involves a standard Holstein-Primakoff transformation

$$S_i^+ = a_i\sqrt{2S - a_i^\dagger a_i}, \quad S_i^z = S - a_i^\dagger a_i\,. \qquad (10)$$

Linear spin-wave theory

The next non-vanishing term in the $1/S$ expansion of (7) beyond $E_{\rm cl}$ is the quadratic Hamiltonian

$$\hat{\mathcal{H}}^{(2)} = JS\sum_{\langle ij\rangle}\Big[a_i^\dagger a_i + \left(\frac{2\lambda-1}{4}\right)\left(a_i^\dagger a_j + a_i^\dagger a_j\right) - i\left(a_i^\dagger a_j - a_j^\dagger a_i\right)\sin\delta\varphi_{ij}\sin\theta + \left(\frac{2\lambda+1}{4}\right)\left(a_i a_j + a_i^\dagger a_j^\dagger\right)\Big], \qquad (11)$$

where $\lambda = \left(\Delta + \frac{1}{2}\right)\cos^2\theta - \frac{1}{2}$. Next, we introduce Fourier transformation

$$a_i = \frac{1}{\sqrt{N}}\sum_{\mathbf{k}} e^{i\mathbf{k}\mathbf{r}_i} a_{\mathbf{k}}\,. \qquad (12)$$

Reciprocal vectors of triangular lattice are

$$\mathbf{b}_1 = \left(0, \frac{4\pi}{\sqrt{3}}\right), \ \mathbf{b}_2 = \left(2\pi, -\frac{2\pi}{\sqrt{3}}\right). \qquad (13)$$

This gives the harmonic Hamiltonian

$$\hat{\mathcal{H}}^{(2)} = 3JS\sum_{\mathbf{k}}\left(A_{\mathbf{k}} + C_{\mathbf{k}}\right)a_{\mathbf{k}}^\dagger a_{\mathbf{k}} - \frac{B_{\mathbf{k}}}{2}\left(a_{\mathbf{k}}^\dagger a_{-\mathbf{k}}^\dagger + \text{H.c.}\right), \qquad (14)$$

with the parameters

$$A_{\mathbf{k}} = 1 + \gamma_{\mathbf{k}}\left[\left(\Delta + \frac{1}{2}\right)\cos^2\theta - 1\right], \qquad (15)$$

$$B_{\mathbf{k}} = -\gamma_{\mathbf{k}}\left(\Delta + \frac{1}{2}\right)\cos^2\theta, \qquad (16)$$

$$C_{\mathbf{k}} = \sqrt{3}\bar{\gamma}_{\mathbf{k}}\sin\theta\,. \qquad (17)$$

Here $\gamma_{\mathbf{k}}$ and $\bar{\gamma}_{\mathbf{k}}$ are the nearest-neighbor amplitudes

$$\gamma_{\mathbf{k}} = \frac{1}{6}\sum_{\boldsymbol{\delta}_i} e^{i\mathbf{k}\cdot\boldsymbol{\delta}_i}, \ \bar{\gamma}_{\mathbf{k}} = \frac{1}{6}\sum_{\boldsymbol{\delta}_i}\text{sign}(\sin\delta\varphi_{ij})\, e^{i\mathbf{k}\cdot\boldsymbol{\delta}_i}, \qquad (18)$$

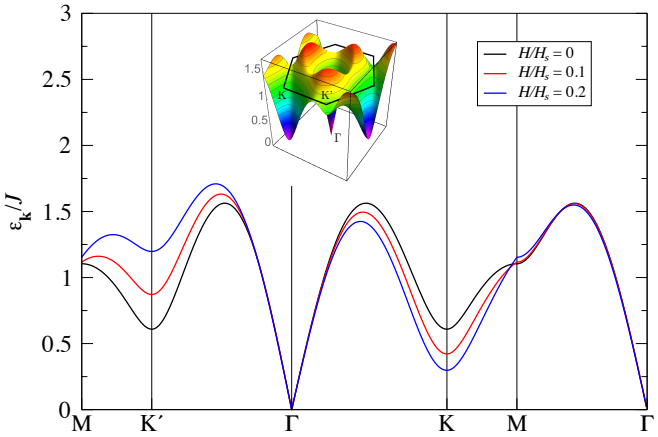

FIG. 2: Magnon linear spin-wave spectrum for $\Delta = 0.9$ and several fields. Inset: 3D plot of $\varepsilon_{\mathbf{k}}$ for $H = 0.2H_s$.

or, explicitly,

$$\gamma_{\mathbf{k}} = \frac{1}{3}\Big(\cos k_x + 2\cos\frac{k_x}{2}\cos\frac{\sqrt{3}k_y}{2}\Big), \qquad (19)$$

$$\bar{\gamma}_{\mathbf{k}} = \frac{1}{3}\Big(\sin k_x - 2\sin\frac{k_x}{2}\cos\frac{\sqrt{3}k_y}{2}\Big). \qquad (20)$$

The Bogolyubov transformation of (11)

$$c_{\mathbf{k}} = u_{\mathbf{k}}a_{\mathbf{k}} + v_{\mathbf{k}}a_{-\mathbf{k}}^\dagger\,, \qquad (21)$$

is standard with the parameters given by

$$2u_{\mathbf{k}}v_{\mathbf{k}} = \frac{B_{\mathbf{k}}}{\sqrt{A_{\mathbf{k}}^2 - B_{\mathbf{k}}^2}}\,, \quad u_{\mathbf{k}}^2 + v_{\mathbf{k}}^2 = \frac{A_{\mathbf{k}}}{\sqrt{A_{\mathbf{k}}^2 - B_{\mathbf{k}}^2}}\,. \qquad (22)$$

Finally, the excitation spectrum is

$$\varepsilon_{\mathbf{k}} = 3JS\omega_{\mathbf{k}}, \qquad (23)$$

where $\omega_{\mathbf{k}} = \sqrt{A_{\mathbf{k}}^2 - B_{\mathbf{k}}^2} + C_{\mathbf{k}}$. Note that because $C_{-\mathbf{k}} = -C_{\mathbf{k}}$, it is not affected by Bogolyubov transformation and $u_{\mathbf{k}}$ and $v_{\mathbf{k}}$ remain even under $\mathbf{k} \to -\mathbf{k}$. Fig. 2 shows the linear spin-wave theory spectra in the range of parameters applicable to $Ba_3CoSb_2O_9$. Since the field-induced staggered scalar chirality of the umbrella structure, $\mathbf{S}_i \cdot (\mathbf{S}_j \times \mathbf{S}_k)$, breaks the inversion symmetry, it leads to an asymmetry of the spectrum [4], $\varepsilon_{\mathbf{k}} \neq \varepsilon_{-\mathbf{k}}$. Most importantly, it shifts magnon energy at K and K′ corners of the Brillouin zone in the opposite directions.

Cubic vertices

Holstein-Primakoff transformation in (8) yields the three-magnon interaction

$$\hat{\mathcal{H}}^{(3)} = J\sqrt{\frac{S}{2}}\sum_{\langle ij\rangle}\sin 2\theta\left(\Delta + \frac{1}{2}\right)(a_i^\dagger + a_i)a_j^\dagger a_j - 2i\cos\theta\sin\delta\varphi_{ij}\, a_i^\dagger a_i(a_j^\dagger - a_j), \qquad (24)$$

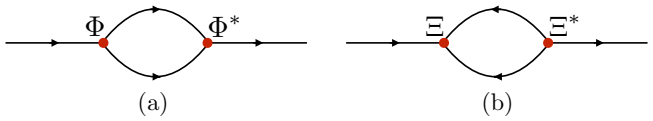

FIG. 3: Decay (a) and source (b) diagrams.

where the first term is due to the out-of-plane spin non-collinearity and the second is due to the 120° in-plane order. The Fourier transformation of (24) yields

$$\hat{\mathcal{H}}^{(3)} = 3J\sqrt{\frac{S}{2}}\sum_{\mathbf{k},\mathbf{q}}\left[\gamma_{\mathbf{k}}\left(\Delta+\frac{1}{2}\right)\sin 2\theta - \sqrt{3}\bar{\gamma}_{\mathbf{k}}\cos\theta\right] \times\left(a^{\dagger}_{\mathbf{q}}a^{\dagger}_{\mathbf{k}}a_{\mathbf{k}+\mathbf{q}}+\text{H.c.}\right). \quad (25)$$

Finally, the Bogolyubov transformation (21) of (25) yields the cubic Hamiltonian for the magnon eigenmodes

$$\hat{\mathcal{H}}^{(3)} = \frac{3J}{3!}\sqrt{\frac{S}{2}}\sum_{-\mathbf{p}=\mathbf{k}+\mathbf{q}}\left(\Xi_{\mathbf{qkp}}c^{\dagger}_{\mathbf{q}}c^{\dagger}_{\mathbf{k}}c^{\dagger}_{\mathbf{p}}+\text{H.c.}\right), \quad (26)$$

$$+\frac{3J}{2!}\sqrt{\frac{S}{2}}\sum_{-\mathbf{p}=\mathbf{k}+\mathbf{q}}\left(\Phi_{\mathbf{qk;p}}c^{\dagger}_{\mathbf{q}}c^{\dagger}_{\mathbf{k}}c_{-\mathbf{p}}+\text{H.c.}\right), \quad (27)$$

where the combinatorial factors are due to symmetrization in the source (26) and decay (27) vertices given by

$$\begin{aligned}\Xi_{\mathbf{qkp}} &= F_{\mathbf{q}}(u_{\mathbf{q}}+v_{\mathbf{q}})(u_{\mathbf{k}}v_{\mathbf{p}}+v_{\mathbf{k}}u_{\mathbf{p}})\\ &+F_{\mathbf{k}}(u_{\mathbf{k}}+v_{\mathbf{k}})(u_{\mathbf{q}}v_{\mathbf{p}}+v_{\mathbf{q}}u_{\mathbf{p}})\\ &+F_{\mathbf{p}}(u_{\mathbf{p}}+v_{\mathbf{p}})(u_{\mathbf{q}}v_{\mathbf{k}}+v_{\mathbf{q}}u_{\mathbf{k}})\\ &+\bar{F}_{\mathbf{q}}(u_{\mathbf{q}}-v_{\mathbf{q}})(u_{\mathbf{k}}v_{\mathbf{p}}+v_{\mathbf{k}}u_{\mathbf{p}})\\ &+\bar{F}_{\mathbf{k}}(u_{\mathbf{k}}-v_{\mathbf{k}})(u_{\mathbf{q}}v_{\mathbf{p}}+v_{\mathbf{q}}u_{\mathbf{p}})\\ &+\bar{F}_{\mathbf{p}}(u_{\mathbf{p}}-v_{\mathbf{p}})(u_{\mathbf{q}}v_{\mathbf{k}}+v_{\mathbf{q}}u_{\mathbf{k}}),\end{aligned} \quad (28)$$

$$\begin{aligned}\Phi^{\eta\nu\mu}_{\mathbf{qk;p}} &= F_{\mathbf{q}}(u_{\mathbf{q}}+v_{\mathbf{q}})(u_{\mathbf{k}}u_{\mathbf{p}}+v_{\mathbf{k}}v_{\mathbf{p}})\\ &+F_{\mathbf{k}}(u_{\mathbf{k}}+v_{\mathbf{k}})(u_{\mathbf{q}}u_{\mathbf{p}}+v_{\mathbf{q}}v_{\mathbf{p}})\\ &+F_{\mathbf{p}}(u_{\mathbf{p}}+v_{\mathbf{p}})(u_{\mathbf{q}}v_{\mathbf{k}}+v_{\mathbf{q}}u_{\mathbf{k}})\\ &+\bar{F}_{\mathbf{q}}(u_{\mathbf{q}}-v_{\mathbf{q}})(u_{\mathbf{k}}u_{\mathbf{p}}+v_{\mathbf{k}}v_{\mathbf{p}})\\ &+\bar{F}_{\mathbf{k}}(u_{\mathbf{k}}-v_{\mathbf{k}})(u_{\mathbf{q}}u_{\mathbf{p}}+v_{\mathbf{q}}v_{\mathbf{p}})\\ &-\bar{F}_{\mathbf{p}}(u_{\mathbf{p}}-v_{\mathbf{p}})(u_{\mathbf{q}}v_{\mathbf{k}}+v_{\mathbf{q}}u_{\mathbf{k}}),\end{aligned} \quad (29)$$

with $\mathbf{k}\leftrightarrow-\mathbf{k}$ symmetric and antisymmetric amplitudes

$$F_{\mathbf{k}} = \gamma_{\mathbf{k}}\left(\Delta+\frac{1}{2}\right)\sin 2\theta, \quad (30)$$

$$\bar{F}_{\mathbf{k}} = -\sqrt{3}\bar{\gamma}_{\mathbf{k}}\cos\theta. \quad (31)$$

The terms with $\bar{F}_{\mathbf{k}}$ in the vertices have a structure familiar from the zero-field consideration [2], while the symmetric terms are from the out-of-plane canting.

Magnon decays

Using standard diagrammatic rules, the one-loop decay and source diagrams shown in Fig. 3 are

$$\Sigma^{(a)}_{11}(\mathbf{k},\omega) = \frac{9J^2S}{4}\sum_{\mathbf{q}}\frac{\left|\Phi_{\mathbf{q},\mathbf{k}-\mathbf{q};\mathbf{k}}\right|^2}{\omega-\varepsilon_{\mathbf{q}}-\varepsilon_{\mathbf{k}-\mathbf{q}}+i\delta}, \quad (32)$$

$$\Sigma^{(b)}_{11}(\mathbf{k},\omega) = -\frac{9J^2S}{4}\sum_{\mathbf{q}}\frac{\left|\Xi_{\mathbf{q},-\mathbf{k}-\mathbf{q},\mathbf{k}}\right|^2}{\omega+\varepsilon_{\mathbf{q}}+\varepsilon_{-\mathbf{k}-\mathbf{q}}-i\delta}. \quad (33)$$

In our numerical calculations we used $\delta = 0.0005J$.

The on-shell magnon decay rate from $\text{Im}\Sigma^{(a)}_{11}$ in (32) is

$$\Gamma_{\mathbf{k}} = \Gamma_0\sum_{\mathbf{q}}\left|\Phi_{\mathbf{q},\mathbf{k}-\mathbf{q};\mathbf{k}}\right|^2\delta\left(\omega_{\mathbf{k}}-\omega_{\mathbf{q}}-\omega_{\mathbf{k}-\mathbf{q}}\right), \quad (34)$$

with the auxiliary constant $\Gamma_0 = 3\pi J/4$.

To get a qualitative insight into magnon decays, one can neglect for a moment the other $1/S$-contributions to the spectrum and focus on the effect of the decay part. Given the field-induced asymmetry of the spectrum, it is clear that the K′ point will be prone to decays above a threshold field. Our Fig. 4 shows the on-shell $\Gamma_{\mathbf{k}}$ from (34) vs H for this representative $\mathbf{k}$-point at several values of Δ. One can see that at large anisotropies, the on-shell damping reaches unphysically large values.

Kinematics.—A more systematic approach to the on-shell decays involves a consideration of the general decay conditions [7], $\varepsilon_{\mathbf{k}} = \varepsilon_{\mathbf{q}}+\varepsilon_{\mathbf{k}-\mathbf{q}}$. The results are presented in the H–Δ diagram in Fig. 5. There are two main decay channels here. First, the threshold field value for decays in the proximity of K′ was found numerically (blue line). However, for $\Delta\lesssim 0.7$ it becomes precisely the threshold condition for the decays directly from the K′ point into two magnons at the equivalent K points: $\varepsilon_{\text{K}'} = 2\varepsilon_{\text{K}}$, which is given analytically by $H^* = \sqrt{(1-\Delta)/(13-\Delta)}$ (dashed line). Note that this channel is permitted by the commensurability of the umbrella state, which retains

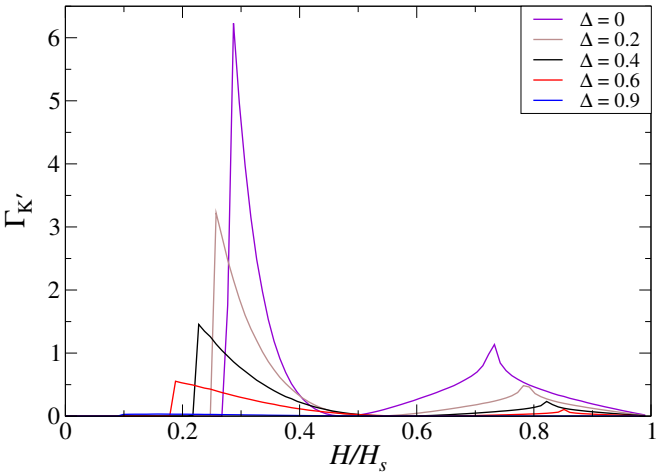

FIG. 4: The on-shell $\Gamma_{\mathbf{k}}$ at the K′ point vs field for several Δ.

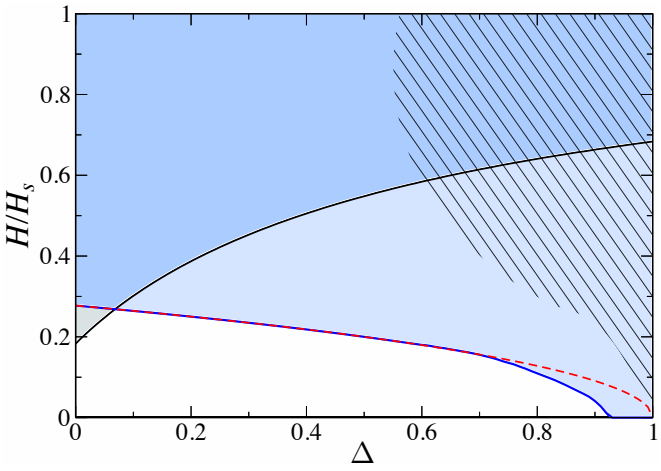

FIG. 5: The H–Δ diagram of the decay thresholds in the umbrella state. Color shaded regions represent values of parameters where decays are allowed by kinematic conditions. The decay condition $\varepsilon_{\mathbf{K}'} = 2\varepsilon_{\mathbf{K}}$ is shown by the dashed line. Decays from a vicinity of the K′ point exist above the blue line. Decays near the Γ point, due to the change of curvature of the Goldstone mode, exist above the black line. For $\Delta > 0.92$ decays exist in zero field [2]. While semiclassically the umbrella state is stable for any $\Delta < 1$, quantum fluctuations lead to proliferation of coplanar states. The non-umbrella region for $S = 1/2$ is sketched from Ref. [6] by a striped pattern.

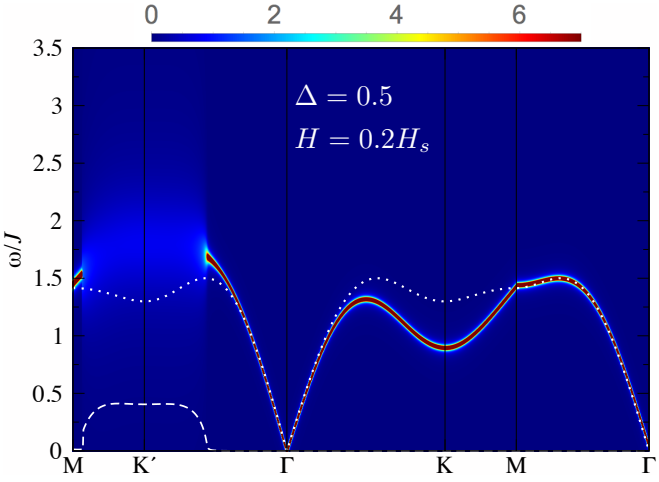

FIG. 6: Intensity plot of the magnon spectral function along the MK′ΓKMΓ path with the iDE $\Gamma_{\mathbf{k}}$, shown by the dashed line. $S = 1/2$, $H = 0.2H_s$, and $\Delta = 0.5$. Dotted line is the LSW spectrum for $H = 0$.

the $3\mathbf{K} = 0$ property of the 120° structure. The second channel is due to the change of curvature of the spectrum to a negative one in the vicinity of the Γ point [3, 8]. Expansion of the spectrum to k^3 order yields

$$\varepsilon_{|\mathbf{k}|\to 0} \simeq \sqrt{\frac{\lambda}{2}}|\mathbf{k}| - |\mathbf{k}|^3 \left[\frac{1}{16}\sqrt{\frac{\lambda}{2}}\left(\frac{5}{2} - \frac{1}{\lambda}\right) + \frac{h\sqrt{3}}{24}\cos 3\phi\right], \tag{35}$$

where $\phi = \tan^{-1}(k_y/k_x)$. The solution of that implicit equation is shown in Fig. 5 as a black line.

Dyson's equation.—In addition to the on-shell damping, one can employ a straightforward self-consistent approach, which we refer to as iDE, which consists of solving the off-shell Dyson's equation (DE) for $\Gamma_{\mathbf{k}}$ of the magnon pole of the Green's function where only the imaginary part of the the magnon self-energy is retained [2]

$$\Gamma_{\mathbf{k}} = -\mathrm{Im}\,\Sigma_{\mathbf{k}}\left(\varepsilon_{\mathbf{k}} + i\Gamma_{\mathbf{k}}\right). \tag{36}$$

This method accounts for a damping of the decaying initial-state magnon and regularizes singularities due to two-magnon continuum. We present some of the results of this approach in Fig. 6, which shows the magnon spectral function (intensity map) with the broadening $\Gamma_{\mathbf{k}}$ (dashed line) for representative field and Δ. The self-consistency clearly mitigates the unphysically large values of the on-shell $\Gamma_{\mathbf{k}}$, but its values remain quite significant. Note that in the iDE self-consistent solution, decays occur at a lower field than suggested by the on-shell consideration.

Altogether, both the on-shell and the iDE considerations suggest a significant field-induced broadening of quasiparticle peaks due to magnon decays in modest fields in a wide vicinity of the K′ points.

Hartree-Fock corrections

For a more consistent consideration of the ω-dependence of the magnon spectral function we also need to include all contributions to the one-loop magnon self-energy of the same $1/S$-order [7]. For that we need the source diagram (33) and the Hartree-Fock corrections. There are two contributions to the latter. First is from the four-magnon interactions (quartic terms) and the second is from the cubic terms due to quantum corrections to the out-of-plane canting angle of spins.

Four magnon interaction terms originate from (7) and can be decoupled using Hartree-Fock averages

$$n = \langle a_i^\dagger a_i\rangle = \sum_{\mathbf{k}} v_{\mathbf{k}}^2, \tag{37}$$

$$m = \langle a_i^\dagger a_j\rangle = \sum_{\mathbf{k}} v_{\mathbf{k}}^2\gamma_{\mathbf{k}}, \tag{38}$$

$$\delta = \langle a_i a_i\rangle = \sum_{\mathbf{k}} u_{\mathbf{k}}v_{\mathbf{k}}, \tag{39}$$

$$\bar{\Delta} = \langle a_i a_j\rangle = \sum_{\mathbf{k}} u_{\mathbf{k}}v_{\mathbf{k}}\gamma_{\mathbf{k}}, \tag{40}$$

to obtain correction to the magnon energy spectrum after decoupling and Fourier transformation

$$\delta\mathcal{H}_2^{(4)} = 3J\sum_{\mathbf{k}}\left(\delta A_{\mathbf{k}}^{(4)} + \delta C_{\mathbf{k}}^{(4)}\right)a_{\mathbf{k}}^\dagger a_{\mathbf{k}} - \frac{\delta B_{\mathbf{k}}^{(4)}}{2}\left(a_{\mathbf{k}}^\dagger a_{-\mathbf{k}}^\dagger + \mathrm{H.c.}\right), \tag{41}$$

where the coefficients are given by

$$\begin{aligned}
\delta A_{\mathbf{k}}^{(4)} &= -d_1 - \gamma_{\mathbf{k}} d_2 \\
d_1 &= \left[\bar{\Delta}\left(\Delta+\frac{1}{2}\right) + m\left(\Delta-\frac{1}{2}\right)+n\right] \\
&\quad -h^2\left(\Delta+\frac{1}{2}\right)\left(2n+\bar{\Delta}+m\right) \\
d_2 &= \left[m+n\left(\Delta-\frac{1}{2}\right)+\frac{\delta}{2}\left(\Delta+\frac{1}{2}\right)\right] \\
&\quad -h^2\left(\Delta+\frac{1}{2}\right)\left(2m+\frac{\delta}{2}+n\right), \qquad (42) \\
\delta B_{\mathbf{k}}^{(4)} &= d_3 + \gamma_{\mathbf{k}} d_4 \\
d_3 &= \frac{1}{2}\left[m\left(\Delta+\frac{1}{2}\right)+\bar{\Delta}\left(\Delta-\frac{1}{2}\right)\right] \\
&\quad -\frac{h^2}{2}\left(\Delta+\frac{1}{2}\right)\left(\bar{\Delta}+m\right) \\
d_4 &= \left[\bar{\Delta}+n\left(\Delta+\frac{1}{2}\right)+\frac{\delta}{2}\left(\Delta-\frac{1}{2}\right)\right] \\
&\quad -h^2\left(\Delta+\frac{1}{2}\right)\left(n+2\bar{\Delta}+\frac{\delta}{2}\right) \qquad (43) \\
\delta C_{\mathbf{k}}^{(4)} &= -\sqrt{3}nh\bar{\gamma}_{\mathbf{k}} \qquad (44)
\end{aligned}$$

and we have introduced a notation $h=\sin\theta$. Using Bogolyubov transformation (21) in this Hamiltonian gives

$$\delta\mathcal{H}_2^{(4)} = \sum_{\mathbf{k}} \varepsilon_{\mathbf{k}}^{(4)} c_{\mathbf{k}}^\dagger c_{\mathbf{k}} - \frac{V_{\mathbf{k}}^{od,(4)}}{2}\left(c_{\mathbf{k}}^\dagger c_{-\mathbf{k}}^\dagger + \text{H.c.}\right), \quad (45)$$

where

$$\varepsilon_{\mathbf{k}}^{(4)} = 3J\left(\frac{A_{\mathbf{k}}\delta A_{\mathbf{k}}^{(4)} - B_{\mathbf{k}}\delta B_{\mathbf{k}}^{(4)}}{\sqrt{A_{\mathbf{k}}^2 - B_{\mathbf{k}}^2}} + \delta C_{\mathbf{k}}^{(4)}\right), \quad (46)$$

$$V_{\mathbf{k}}^{od,(4)} = -3J\,\frac{B_{\mathbf{k}}\delta A_{\mathbf{k}}^{(4)} - A_{\mathbf{k}}\delta B_{\mathbf{k}}^{(4)}}{\sqrt{A_{\mathbf{k}}^2 - B_{\mathbf{k}}^2}}, \quad (47)$$

and $\delta C_{\mathbf{k}}^{(4)}$ is not affected by diagonalization as it is odd in $\mathbf{k}$. Thus, the Hartree-Fock corrections from the four-magnon interaction to the energy spectrum is $\varepsilon_{\mathbf{k}}^{(4)}$.

Quantum correction from the three-boson terms

The Hartree-Fock decoupling of the three-magnon term (24) gives a correction to the canting angle θ via

$$\hat{\mathcal{H}}^{(1)} + \hat{\mathcal{H}}_1^{(3)} = (V_1 + \delta V_1)\sum_i\left(a_i + a_i^\dagger\right), \quad (48)$$

where $\delta V_1 = 3J\sqrt{S/2}(\Delta+1/2)\sin 2\theta(\bar{\Delta}+m+n)$, adding to the contribution of the Hamiltonian in (8), $\hat{\mathcal{H}}^{(1)}$, which was vanishing due to energy minimization, with $V_1 = \sqrt{S/2}\cos\theta\,(H - 6JS\sin\theta\,(\Delta+1/2))$. Now, both terms should be (re)balanced to zero: $\delta\hat{\mathcal{H}}_1^{(3)} + \delta\hat{\mathcal{H}}^{(1)} = 0$, giving the $1/S$ correction to the canting angle [3]

$$\delta\theta = \frac{\sin\theta_0\left(\bar{\Delta}+m+n\right)}{S\cos\theta_0}, \quad (49)$$

or, using $1/S \ll 1$,

$$\sin\theta = \sin\theta_0\left(1+\frac{\bar{\Delta}+m+n}{S}\right). \quad (50)$$

This yields a correction to the harmonic term (11)

$$\delta\hat{\mathcal{H}}_2^{(3)} = \frac{\partial\hat{\mathcal{H}}^{(2)}}{\partial\theta}\delta\theta, \quad (51)$$

which, after Fourier transform, can be written as

$$\begin{aligned}
\delta\hat{\mathcal{H}}_2^{(3)} = 3JS\sum_{\mathbf{k}}&\left(\delta A_{\mathbf{k}}^{(3)} + \delta C_{\mathbf{k}}^{(3)}\right)a_{\mathbf{k}}^\dagger a_{\mathbf{k}} \qquad (52)\\
&- \frac{\delta B_{\mathbf{k}}^{(3)}}{2}\left(a_{\mathbf{k}}^\dagger a_{-\mathbf{k}}^\dagger + \text{H.c.}\right),
\end{aligned}$$

with the parameters given by

$$\delta A_{\mathbf{k}}^{(3)} = -\left(1+\gamma_{\mathbf{k}}\right)\left(\Delta+\frac{1}{2}\right)\sin 2\theta\cdot\delta\theta, \quad (53)$$

$$\delta B_{\mathbf{k}}^{(3)} = \gamma_{\mathbf{k}}\left(\Delta+\frac{1}{2}\right)\sin 2\theta\cdot\delta\theta, \quad (54)$$

$$\delta C_{\mathbf{k}}^{(3)} = \sqrt{3}\bar{\gamma}_{\mathbf{k}}\cos\theta\cdot\delta\theta. \quad (55)$$

Similarly to the quartic terms (45), this gives

$$\varepsilon_{\mathbf{k}}^{(3)} = 3JS\left(\frac{A_{\mathbf{k}}\delta A_{\mathbf{k}}^{(3)} - B_{\mathbf{k}}\delta B_{\mathbf{k}}^{(3)}}{\sqrt{A_{\mathbf{k}}^2 - B_{\mathbf{k}}^2}} + \delta C_{\mathbf{k}}^{(3)}\right), \quad (56)$$

$$V_{\mathbf{k}}^{od,(3)} = -3JS\left(\frac{B_{\mathbf{k}}\delta A_{\mathbf{k}}^{(3)} - A_{\mathbf{k}}\delta B_{\mathbf{k}}^{(3)}}{\sqrt{A_{\mathbf{k}}^2 - B_{\mathbf{k}}^2}}\right). \quad (57)$$

Altogether, the Hartree-Fock correction to the magnon energy spectrum is given by

$$\Sigma^{\text{HF}}(\mathbf{k}) = \varepsilon_{\mathbf{k}}^{(3)} + \varepsilon_{\mathbf{k}}^{(4)}. \quad (58)$$

Magnon spectral function

The spectral function, $A(\mathbf{k},\omega) = -\frac{1}{\pi}\text{Im}G(\mathbf{k},\omega)$, with the Green's function $G(\mathbf{k},\omega) = [\omega - \varepsilon_{\mathbf{k}} - \Sigma(\mathbf{k},\omega) + i\delta]^{-1}$, can now be calculated using the full expression for the $1/S$, one-loop, ω-dependent self-energy (32), (33), (58)

$$\Sigma(\mathbf{k},\omega) = \Sigma^{\text{HF}}(\mathbf{k}) + \Sigma_{11}^{(a)}(\mathbf{k},\omega) + \Sigma_{11}^{(b)}(\mathbf{k},\omega). \quad (59)$$

In our calculations, we also kept the source self-energy term on-shell, i.e., $\Sigma_{11}^{(b)}(\mathbf{k},\varepsilon_{\mathbf{k}})$, in order to avoid interaction with negative frequency excitations, see [5].

The results of the calculations of the spectral function $A(\mathbf{k},\omega)$ are shown as intensity plots in Fig. 7(a)-(c) for

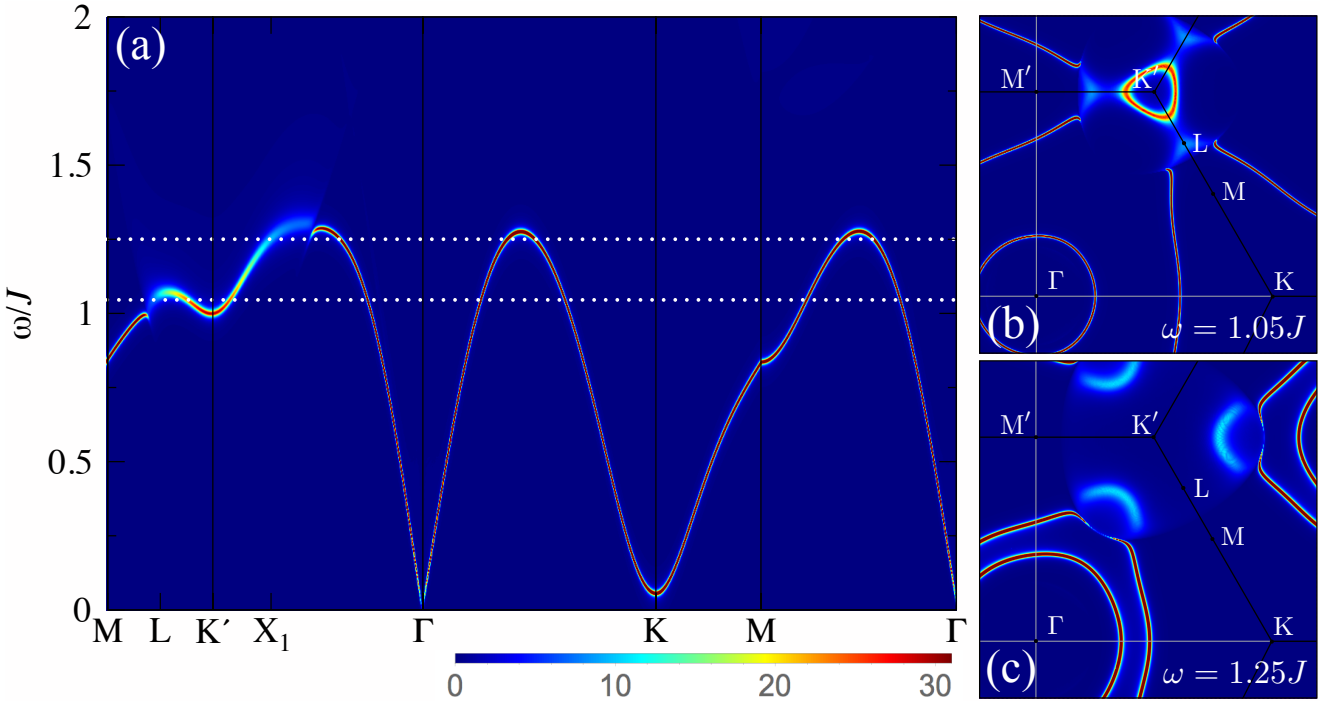

FIG. 7: (a) The $\mathbf{k}-\omega$ intensity plot of the spectral function $A(\mathbf{k},\omega)$ along the MK′ΓKMΓ path. Dotted lines indicate constant energy cuts in (b) and (c), where intensity plots at $\omega = 1.05J$ and $\omega = 1.25J$ are shown. $S = 1/2$, $\Delta = 0.9$, $H = 0.2H_s$.

$S = 1/2$, $\Delta = 0.9$, and $H = 0.2H_s$. A cut along the high-symmetry path in Fig. 7(a) exhibits a strong spectrum renormalization, $\sim 30\%$, and a significant broadening of the quasiparticle peaks for an extensive range of momenta in the vicinity of K′ corners of the BZ. The latter is due to an overlap of the one-magnon spectrum with the two-magnon continuum associated with the roton-like excitations at the K points. One can also see well-pronounced termination points with distinctive bending of spectral lines and other non-Lorentzian features in Fig. 7(a). The 2D intensity maps of the constant-energy cuts of $A(\mathbf{k},\omega)$ at $\omega = 1.05J$ and $\omega = 1.25J$ are shown in Fig. 7(b) and (c), where one can see multiple signatures of the broadening, spectral weight redistribution, and termination points.

Dynamical structure factor

We approximate the dynamical structure factor [5] as a sum of the diagonal terms of

$$\mathcal{S}^{\alpha_0\beta_0}(\mathbf{q},\omega) = \frac{i}{\pi}\mathrm{Im}\int_{-\infty}^{\infty} dt e^{i\omega t}\langle T S^{\alpha_0}_{\mathbf{q}}(t) S^{\beta_0}_{-\mathbf{q}}(0)\rangle. \quad (60)$$

The spin rotation to the local reference frame yields (keeping the leading $1/S$ terms)

$$\mathcal{S}^{x_0x_0}(\mathbf{q},\omega) = \frac{1}{4}\Big[\left(\mathcal{S}^{yy}_{\mathbf{q}+} + \mathcal{S}^{yy}_{\mathbf{q}-}\right) - 2i\sin\theta\left(\mathcal{S}^{xy}_{\mathbf{q}+} - \mathcal{S}^{xy}_{\mathbf{q}-}\right) + \sin^2\theta\left(\mathcal{S}^{xx}_{\mathbf{q}+} + \mathcal{S}^{xx}_{\mathbf{q}-}\right) + \cos^2\theta\left(\mathcal{S}^{zz}_{\mathbf{q}+} + \mathcal{S}^{zz}_{\mathbf{q}-}\right)\Big], \quad (61)$$

$$\mathcal{S}^{y_0y_0}(\mathbf{q},\omega) = \mathcal{S}^{x_0x_0}(\mathbf{q},\omega), \quad (62)$$

$$\mathcal{S}^{z_0z_0}(\mathbf{q},\omega) = \cos^2\theta\,\mathcal{S}^{xx}_{\mathbf{q}} + \sin^2\theta\,\mathcal{S}^{zz}_{\mathbf{q}}, \quad (63)$$

where we used $\mathcal{S}^{xy}_{\mathbf{q}} = -\mathcal{S}^{yx}_{\mathbf{q}}$ and the shorthand notations from Ref. [5], $\mathcal{S}_{\mathbf{q}\pm} \equiv \mathcal{S}(\mathbf{q}\pm\mathbf{Q},\omega)$.

We note that the off-diagonal component, $\mathcal{S}^{x_0y_0}(\mathbf{q},\omega)$, is also non-zero, but its contribution to the total structure factor for an unpolarized beam is canceled exactly by its partner, $\mathcal{S}^{y_0x_0}(\mathbf{q},\omega)$, leaving the $\mathcal{S}^{xy}_{\mathbf{q}\pm}$ contributions in (61) and (62) to be the sole unorthodox terms due to the field-induced chiral structure.

Transverse components of $\mathcal{S}(\mathbf{q},\omega)$ are given by

$$\mathcal{S}^{xx(yy)}_{\mathbf{q}} = \frac{S}{2}\Lambda_{\pm}^2\left(u_{\mathbf{q}} \pm v_{\mathbf{q}}\right)^2 A(\mathbf{q},\omega), \quad (64)$$

$$\mathcal{S}^{xy}_{\mathbf{q}} = i\frac{S}{2}\Lambda_+\Lambda_- A(\mathbf{q},\omega), \quad (65)$$

where $\Lambda_\pm = 1 - (2n \pm \delta)/4S$, and the longitudinal one is

$$\mathcal{S}^{zz}_{\mathbf{q}} = \frac{1}{2}\sum_{\mathbf{k}}\left(u_{\mathbf{k}}v_{\mathbf{q}-\mathbf{k}} + v_{\mathbf{k}}u_{\mathbf{q}-\mathbf{k}}\right)^2\delta\left(\omega - \varepsilon_{\mathbf{k}} - \varepsilon_{\mathbf{q}-\mathbf{k}}\right). \quad (66)$$

Clearly, $\mathcal{S}(\mathbf{q},\omega)$ should feature three overlapping single-magnon spectral functions, $A(\mathbf{q},\omega)$ and $A(\mathbf{q}\pm\mathbf{Q},\omega)$, with different kinematic formfactors.

In Fig. 8 we present constant energy cuts of $\mathcal{S}(\mathbf{q},\omega)$ at the same energies and parameters as in Fig. 7(b) and (c) to demonstrate proliferation of the unusual features discussed for the spectral function.

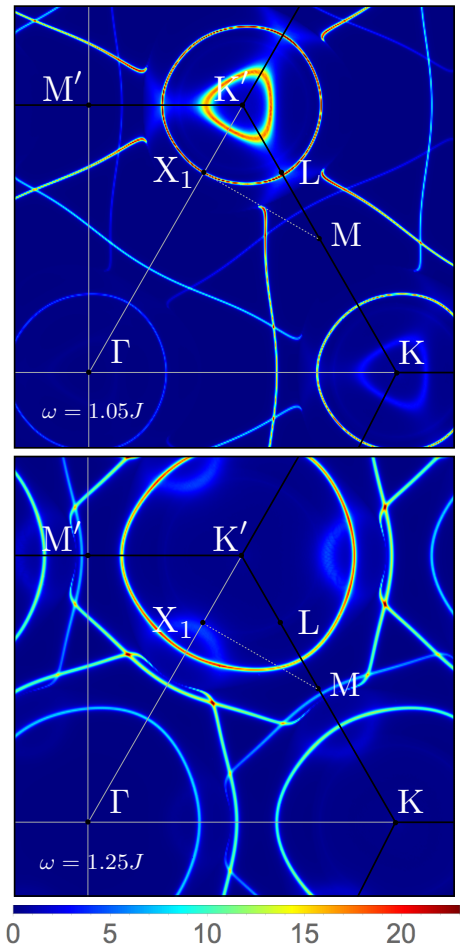

FIG. 8: Intensity plots of the constant energy cuts of $\mathcal{S}(\mathbf{q},\omega)$ at the same ω and parameters as in Fig. 7(b) and (c).

[1] O. A. Starykh, A. V. Chubukov, and A. G. Abanov, Phys. Rev. B 74, 180403 (2006).

[2] A. L. Chernyshev and M. E. Zhitomirsky, Phys. Rev. Lett. **97**, 207202 (2006); Phys. Rev. B **79**, 144416 (2009).

[3] M. E. Zhitomirsky and A. L. Chernyshev, Phys. Rev. Lett. **82**, 4536 (1999); M. Mourigal, M. E. Zhitomirsky, and A. L. Chernyshev, Phys. Rev. B **82**, 144402 (2010); W. T. Fuhrman, M. Mourigal, M. E. Zhitomirsky, and A. L. Chernyshev, Phys. Rev. B **85**, 184405 (2012).

[4] M. E. Zhitomirsky and I. A. Zaliznyak, Phys. Rev. B **53**, 3428 (1996).

[5] M. Mourigal, W. T. Fuhrman, A. L. Chernyshev, and M. E. Zhitomirsky, Phys. Rev. B **88**, 094407 (2013).

[6] D. Yamamoto, G. Marmorini, and I. Danshita, Phys. Rev. Lett. **112**, 127203 (2014); G. Marmorini, D. Yamamoto, and I. Danshita, Phys. Rev. B **93**, 224402 (2016).

[7] M. E. Zhitomirsky and A. L. Chernyshev, Rev. Mod. Phys. **85**, 219 (2013).

[8] L.P. Pitaevskii, Zh. Eksp. Teor. Fiz. **36**, 1168 (1959) [Sov. Phys. JETP **9**, 830 (1959)].